Preparation and Characterization of Polymer-Based Spherical Activated Carbons with Tailored Pore Structure

Zhaolian Zhu, Aimin Li, Sheng Zhong, Fuqiang Liu, Quanxing Zhang

State Key Laboratory of Pollution Control and Resource Reuse, Jiangsu Engineering and Technology Research Center for Organic Toxicant Control and Resource Reuse, School of the Environment, Nanjing University, Nanjing 210093, China

ABSTRACT: A series of spherical activated carbons (SACs) with different pore structure were prepared from divinylbenzene-based polymer through CO_2 activation. The effect of activation temperature and retention time on the yield and textural properties of the resulting SACs were studied. The SACs were characterized by N_2 adsorption, X-ray diffraction, scanning electron microscopy, and aqueous adsorption assays. Either increasing activation temperature or extending retention time decreases the yield of SACs. The BET surface area and pore volume increase with activation temperature and reach a maximum at 1000°C and then decrease at higher activation temperatures. At 1000°C, BET surface area, total pore volume, and mesopore pore volume increase with retention time from 0.5 to 2 h, and meanwhile micropore volume decreases. The micropores are gradually widened into mesopores with increasing activation temperature or extending retention time. SEM and XRD analyses of SAC10 verify the presence of developed porous structure composed of disordered micrographite stacking. Aqueous adsorption assays indicate that SACs have good adsorption capacity for phenol. © 2008 Wiley Periodicals, Inc. J Appl Polym Sci 109: 1692–1698, 2008

Key words: spherical activated carbon; polymer; physical activation; pore structure; adsorption

INTRODUCTION

Activated carbons are widely used as effective adsorbents in many applications such as air separation and purification, pollution control, solvent recovery, catalyst support, and energy storage due to their large specific surface area, adequate pore size distribution, high surface activity, and high physicochemical stability.[1–6]

Activated carbons are usually prepared from organic precursors of natural or synthetic origin by two traditional methods, namely physical activation and chemical activation. Physical activation basically consists of a carbonization step followed by a step of activation by means of air, carbon dioxide or steam. In chemical activation, the carbonization and activation are accomplished in a single step by carrying out thermal decomposition of the raw material impregnated with certain chemical agents (H_3PO_4, $ZnCl_2$, KOH, NaOH, K_2CO_3, etc.).[7]

The use of natural precursors (e.g., wood and coal) will still limit the purity, strength, physical form, and homogeneity of activated carbon. However, these can be fully overcome by the use of polymeric precursors, where the reproducibility and purity of the precursors are within the control of the manufacturer. Meanwhile, the physical forms and structure can be tailored through polymer production process. Many polymers have been studied as activated carbon precursors, such as phenolic resins,[8–12] mixtures of furfuryl resin and glycol,[13] vinylidene chloride copolymer,[14] cellulose based materials,[15] polytetrafluoroethylene,[16] poly(ethyleneterephthalate) and polyacrylonitrile.[17,18]

Activated carbon fibers (ACFs) and granular activated carbons (GACs) are two kinds of the most widely used activated carbon materials. However, spherical activated carbons (SACs) have received considerable recent attention for their various potential advantages over ACFs and GACs such as extremely low resistance to liquid diffusion, higher adsorption efficiency, better mechanical properties, and more resistance to abrasion.[19]

The aim of this study is to prepare and characterize a series of SACs with tailored pore structure derived from divinylbenzene-based polymer through CO_2 activation. The preparation conditions affecting the yield and textural properties (specific surface area, pore volume, and pore size distribution) were

investigated. The textural properties of SACs were characterized by N_2 adsorption, XRD, SEM, and aqueous adsorption assays.

EXPERIMENTAL

SACs preparation

Divinylbenzene-derived spherical polymers (SPs) were synthesized essentially as described.[20] Briefly, styrene (126 g), divinylbenzene (74 g), dibenzoyl peroxide (2 g), and liquid paraffin (100 g) were mixed in a round-bottomed flask. Subsequently, 1200 g of 1 wt % gelatin solution, $MgSO_4$ (92 g), and Na_2CO_3 (28 g) were added. Polymerization was performed with stirring at 80°C for 12 h. When the reaction was completed, SPs were filtered and rinsed with hot deionized water at 80°C, and extracted with acetone for 8 h before being dried under vacuum at 60°C.

The resulting SPs were placed in a quartz combustion boat and loaded into a horizontal cylindrical furnace (i.d. = 80 mm) under N_2 flow (150 cm^3 min^{-1}). After that, the samples were heated up to 700–1100°C for carbonization at a heating rate of 5°C min^{-1} and maintained at the desired carbonization temperature for 1 h. The resulting chars were then activated with CO_2 (250 cm^3 min^{-1}) at the carbonization temperature for 0.5–2 h. The samples prepared at activation temperatures of 700, 800, 900, 1000, and 1100°C for 1 h were designated as SAC7, SAC8, SAC9, SAC10, and SAC11, respectively, and those at 1000°C for 0.5 and 2 h as SAC10-0.5 and SAC10-2. The resultant SACs were washed sequentially with 0.5N HCl solution at 80°C and boiling water to remove residual organic and mineral matters before being dried at 110°C for 24 h and stored in a desiccator for characterization.

SACs characterization

The specific surface area (S_{BET}) and pore structural parameters of the SACs were determined from the adsorption-desorption isotherm of nitrogen at −196°C (Micromeritics ASAP2010). The S_{BET} was calculated by the BET equation, micropore volume (V_{mi}) and micropore specific surface (S_{mi}) area were obtained using the t-plot method, and pore size distribution (PSD) was determined using the BJH model.[21] The total pore volume (V_t) was obtained by converting the nitrogen adsorption amount at a relative pressure of 0.98 to the liquid nitrogen volume. The mesopore volume (V_{me}) was calculated by subtracting V_{mi} from V_t.

The morphology of SAC10 was examined in an SEM (Hitachi S-4300). The SAC10 was coated with platinum by a platinum sputtering device for clear visibility of the surface morphology. The stacking structure of aromatic carbon layers of SAC10 was analyzed with an X-ray diffractometer (ARL-X′ TRA, Cu Ka radiation at 40 kV and 30mA, λ = 0.15,406 nm) and the X-ray patterns were recorded for 2θ from 8 to 60° at a scan rate of 0.02° per min.

Aqueous adsorption characteristics

Activated carbon adsorption is one of the most effective processes for removal of pollutants due to its extraordinary adsorption ability. Phenolic compounds are ubiquitous pollutants in municipal water and industrial effluents. Thus, phenol was chosen as target adsorbate to test the adsorption capability of SACs. The adsorption assays were carried out using a batch equilibration technique in a 250 mL flask. Each flask was filled with 0.05 g SACs and 50 mL of phenol solution at known concentration gradients from 50 to 150 mg L^{-1}. The flasks were shaken in a temperature-controlled shaker at a constant temperature (25°C) and agitation speed (140 rpm) for 4 days to attain equilibrium. The phenol concentration was determined by HPLC (Waters 600, Waters Corp.) using a 30 : 70 ratio of CH_3OH: deionized water and the effluents were monitored at 275 nm; the adsorption capacity was calculated according to $Q_e = (C_0 − C_e)V/W$, where C_0 and C_e are the initial and equilibrium concentrations (mg L^{-1}), respectively; V is the volume (L) and W the weight (g) of SACs.

RESULTS AND DISCUSSION

Yield of SACs

The yield of SACs can be calculated from the resultant sample weight to its initial polymer precursor weight. The effects of activation temperature and retention time on the yield of SACs are shown in Figure 1. For a 1-h activation retention time, as activation temperature increases from 700 to 1100°C, the yield of SACs decreases sharply from 52 to 24% due to the release of volatile matters as well as the gasification reaction between carbon and carbon dioxide. At 1000°C, as activation retention time is extended from 0.5 to 2 h, the yield decreases continually from 31 to 15% as a result of severe gasification reaction. In summary, either increasing activation temperature or extending retention time results in decrease of the yield of SACs.

Nitrogen adsorption-desorption isotherms

Information on the textural properties of porous solids is typically obtained from low-temperature (−196°C) nitrogen adsorption-desorption isotherms. Figure 2(a) shows that the adsorption capacity of SACs increases with activation temperature from 800
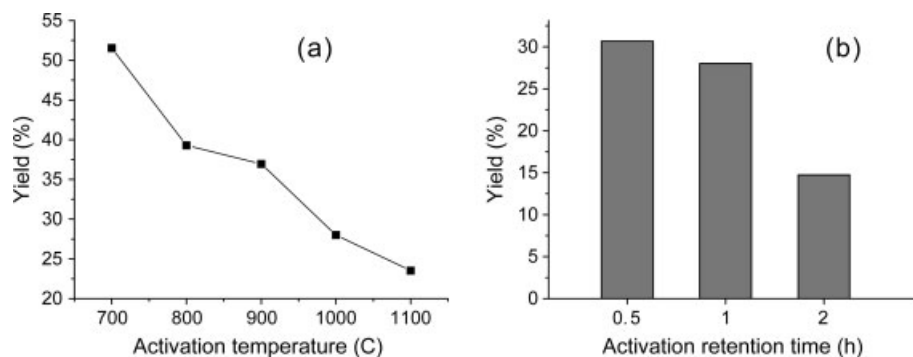
Figure 1 Effects of activation temperature (a) and retention time (b) on yield of the resulting SACs. The retention time in tests for temperature (a) was 1 h; the temperature in tests for retention time (b) was 1000°C.

to 1000°C, indicating the increase of porosity upon activation. It can also be seen that the knees of the isotherms of SACs prepared below 1000°C are sharp and the plateaus are fairly horizontal, which is characteristic of the type I isotherm according to the IUPAC classification, thus the SACs prepared below 1000°C are mainly microporous. For activation at 1000–1100°C, the adsorption capacity of SACs decreases dramatically possibly due to the sintering effect, which seals off some of the pores and reduces the accessibility of the N_2 molecules, and meanwhile widening of the micropores into mesopores, as inferred from the opening of the knee of the isotherm and higher slope of the plateau.[22]

At 1000°C, N_2 adsorption increases with extending retention time from 0.5 to 2 h due to adequate carbon gasification resulting in pore deepening and pore widening. The activation time extended to 2 h, the isotherm of SACs changes from type I to a mixture type of I and IV. Isotherm of type IV originates from mesoporous materials. Therefore, it can be inferred that micropores are gradually formed with activation process and that meanwhile some of them are widened into mesopores. The contribution of

mesopores is clearly reflected by the opening of the knee of the isotherm [Fig. 2(b)].

BET surface area and pore volume

Adsorptive capacity, the most important of SACs properties, is directly related to specific surface area and pore volume. The textural characteristics of SACs are presented in Table I and the effects of activation temperature and retention time on micropore volume fraction (mi%) and mesopore volume fraction (me%) shown in Figure 3. As the activation temperature is 700°C, pyrolysis reaction has just commenced, thereby producing very small surface areas and pore volume due to the inadequacy of heat energy to drive away any substantial amounts of volatiles. As the temperature is increased from 800 to 1000°C, increasingly greater volatile matters are released progressively during activation thereby resulting in the opening up of closed micropores and enlargement of opened micropores, hence S_{BET}, S_{mi}, V_t, V_{mi}, and V_{me} increase progressively. However, further increase in activation temperature results in their decrease, which can be attributed to
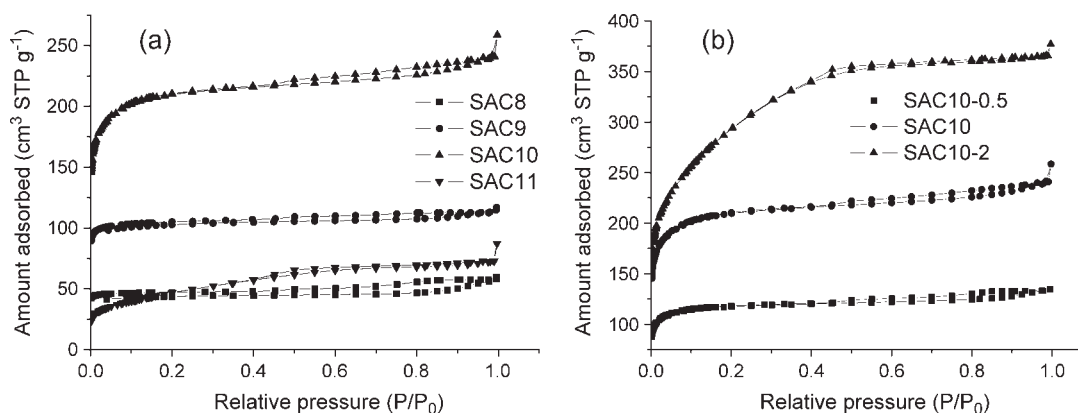

Figure 2 Effects of activation temperature (a) and retention time (b) on the nitrogen adsorption-desorption isotherms of SACs.

TABLE I
The Textural Characteristics of SACs

Sample	S_{BET} $(m^2 g^{-1})$	S_{mi} $(m^2 g^{-1})$	V_t $(cm^3 g^{-1})$	V_{mi} $(cm^3 g^{-1})$	V_{me} $(cm^3 g^{-1})$
SAC7	39	41	0.018	0.019	≈ 0
SAC8	144	123	0.0867	0.0583	0.0284
SAC9	344	299	0.1739	0.1392	0.0347
SAC10	712	534	0.3690	0.2459	0.1231
SAC11	168	20.1	0.1115	0.0074	0.1041
SAC10-0.5	397	328	0.2058	0.1518	0.054
SAC10-2	1043	237	0.5637	0.1000	0.4637

the fact that severe thermal treatment causes sintering and shrinkage of the pore structure. The mi% decreases from about 100 to 7% and me% increases from about zero to 93% with the activation temperature increase from 700 to 1000°C, indicating micropores widened into mesopores upon activation.

At 1000°C, S_{BET}, V_t, and V_{me} increase with retention time extended from 0.5 to 2 h as a result of opening up of closed micropores and enlargement of opened micropores. At the same time S_{mi} and V_{mi} increase with retention time extended from 0.5 to 1 h and thereafter decrease, which can be attributed to the fact that a longer retention time causes destroying of the walls between adjacent pores and micropores widened into mesopores.[23] The mi% decreases from about

74 to 18% and me% increases from about 26 to 82% as a result of the fact that pore-widening effect dominates the process, causing generating micropores widened immediately into mesopores and increase of V_{me} remarkably exceeding decrease of V_{mi}.

Pore size distribution

Pore size distribution (PSD), a very important property of adsorbents, determines the fraction of total pore volume accessible to molecules of a given size and shape. According to the classification adopted by the IUPAC, pores are classified as micropores (<2 nm), mesopores (2–50 nm) and macropores (>50 nm). It is found that increasing activation temperature from 800 to 1000°C results in the enhancement of micropores and mesopores [Fig. 4(a)]. As
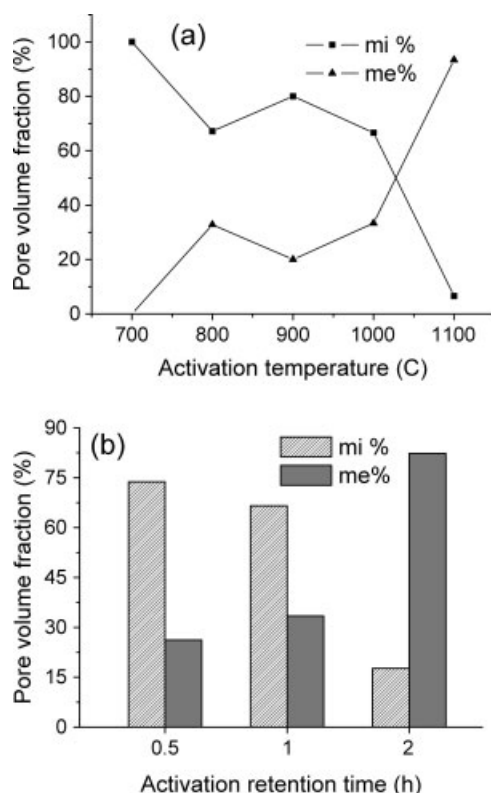
Figure 3 Effects of activation temperature (a) and retention time (b) on evolution of micropre and mesopore volume fraction.
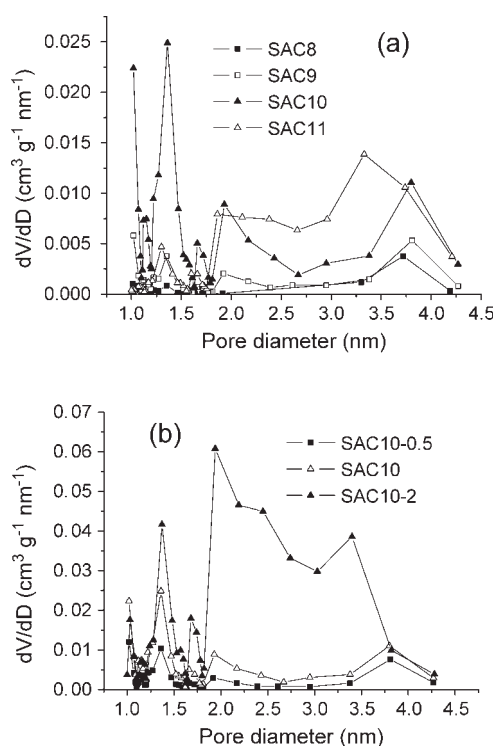
Figure 4 Effects of activation temperature (a) and retention time (b) on PSD of SACs.
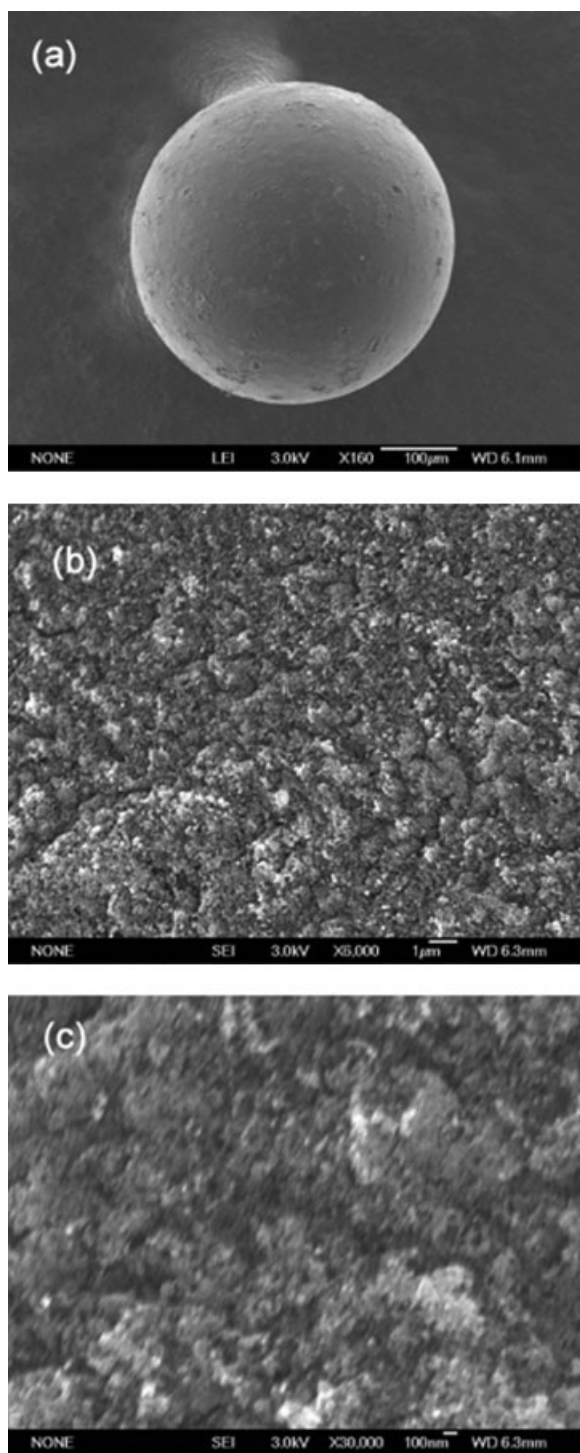
Figure 5 SEM micrographs of SAC10 at different magnification scales. a single sphere magnified 160 times (a), the surface of the sphere magnified 6000 (b), and 30,000 (c) times, respectively.

activation temperature increases from 1000 to 1100°C, micropores decrease and mesopores increase remarkably due to further gasification of labile carbons in the pore walls resulting in the conversion of microporosity into mesoporositiy. Figure 4(b) shows that there are increasing micropores and mesopores

with extending retention time from 0.5 to 2 h. This trend can be explained by the fact that carbon gasification is enhanced by extending activation retention time, thus causing pore deepening and pore widening. The results show that pore structure development can be well tailored by varying the activation temperature and retention time.

Surface morphology

The morphology of SAC10 was detected in a scanning electron microscope (SEM). The surface of SAC10 is magnified 160, 6000, and 30,000 times, respectively, (Fig. 5). The regular spherical shape of the polymer is preserved after activation and there are some shallow cavities at the surface. The micrograph (×6000) shows that there are many fissures and hillocks surrounded with fissures, forming a system of inhomogeneous pore structures. Under higher magnification (×30,000), there are large amounts of interspaces in the order of nanometers, revealing a highly developed disorganized porosity.

Crystal structure

The X-ray diffraction profile of SAC10 (Fig. 6), two very broad diffraction peaks and absence of a sharp peak, reveals a predominantly amorphous structure.[24] There are two peaks centered at around 21.5° and 44.0°, each corresponding to the (002) and (10) (overlapped 100 and 101) reflections of the disordered stacking of micrographites. From the position of the (002) peak, we can calculate an estimate of the interplanar distance (d002) by Bragg's Law. Typically, in a crystalline carbonaceous structure, such as graphite, the interlayer distance between two adjacent carbon sheets is 0.335 nm. In this study, the peak at $2\theta = 21.5°$ corresponds to an interlayer distance (d002) of 0.412 nm, which suggested a disordered carbonaceous interlayer different from that of graphite.[25] The amorphous structure is made up of curved layers of carbon in which the basic building units are distorted six-membered carbon rings. The
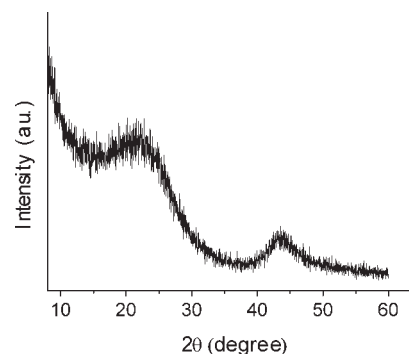

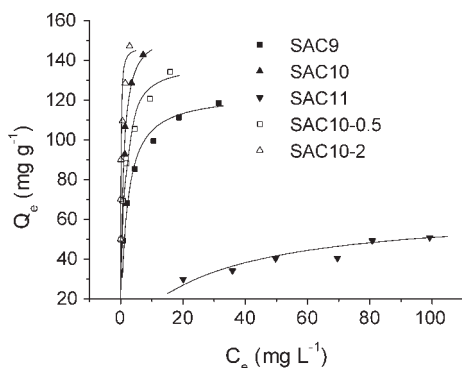**Figure 6** The X-ray diffraction profile of SAC10.

Figure 7 Adsorption isotherms of phenol on SACs. Symbols are the measured values; lines are fits using the Langmuir isotherm.

highly coherent regions are separated by highly defective regions, which provide prerequisites for the realization of a high specific surface area.

Aqueous adsorption characteristics

Adsorption isotherms of phenol on SACs are presented in Figure 7. The adsorption capacities compare fairly well and even favorably with those reported in the literatures for other activated carbons.[7,26–29] The adsorption capacity for phenol decreases in the following order: SAC10-2 > SAC10 > SAC10-0.5 > SAC9 > SAC11, corresponding to the order of the magnitudes of the S_{BET} and V_t presented in Table I. Generally, adsorbents with larger accessible internal surface and pore volume, adsorb more organic molecules. PSD of all SACs mainly concentrates in the range between 1 and 4 nm (Fig. 4), consists of micropores and small mesopores where phenol can enter and adsorb, thus SACs with larger S_{BET} and V_t have larger adsorption capacities for phenol.

To facilitate estimation of the adsorption capacities, two well-known equilibrium adsorption models, Freundlich and Langmuir, are employed.

$$\text{Langmuir equation: } C_e/q_e = 1/K_L q_m + C_e/q_m \quad (1)$$

$$\text{Freundilch equation: } \log q_e = \log K_F + (1/n) \log C_e \quad (2)$$

where C_e is the equilibrium concentration (mg L^{-1}), K_L is the Langmuir constant and q_m is the monolayer adsorption capacity (mg g^{-1}), and K_F and n are the Freundlich constant. Basically, K_L and q_m as well as K_F and n are obtained from linearized plots of C_e/q_e versus C_e and log q_e versus log C_e, respectively.

Table II summarizes the values of the fitting parameters together with the corresponding correlation coefficients. According to the results, adsorption of phenol onto SACs can be better fitted with the Langmuir equation than Freundlich equation. The high correlation coefficients ($R^2 > 0.98$) indicate the applicability of Langmuir equation for adsorption of phenol on SACs. In Langmuir equation, $K_L q_m$ can serve as a measure of the relative adsorptive affinity between the adsorbate and adsorbent. It is in the following order: SAC10-2 > SAC10 > SAC10-0.5 > SAC9 > SAC11, which is in agreement with our previous results.

CONCLUSIONS

Spherical activated carbons (SACs) with tailored pore structures are successfully prepared from divinylbenzene-based spherical polymer through CO_2 activation. Activation temperature and retention time play an important role on the surface areas and porosities of the resulting SACs. Increasing the activation temperature or extending retention time decreases the yield of SACs. S_{BET}, S_{mi}, V_t, V_{mi} and V_{me} increase with activation temperature from 700 to 1000°C due to the creation of new pores and widening of existing pores, and thereafter decrease due to excessive burn-off of carbon constituents causing sintering and shrinkage of the pore structure. SACs preprared below 1000°C are mainly microporous. At 1000°C, S_{BET}, V_t, and V_{me} increase with retention time extended from 0.5 to 2 h as a result of opening up of closed micropores and enlargement of opened micropores. At the same time S_{mi} and V_{mi} increase with retention time extended from 0.5 to 1 h and thereafter decrease, which can be attributed to the fact that a longer retention time causes destroying of the walls between adjacent pores and micropores widened into mesopores. The pore structure development of SACs can be well tailored by controlling

TABLE II
Adsorption Isotherms Fitting Parameters of SACs

SACs	Langmuir				Freundlich		
	q_m (mg g^{-1})	K_L	$K_L q_m$	R^2	K_F	n	R^2
SAC9	123.5	0.55	67.9	0.998	56.0	4.28	0.976
SAC10	156.3	1.33	207.9	0.997	81.6	3.04	0.953
SAC11	65.4	0.035	2.29	0.988	9.99	2.81	0.981
SAC10-0.5	138.9	1.07	148.6	0.995	72.5	4.27	0.988
SAC10-2	147.1	13.6	2001	0.992	123.6	8.16	0.978

activation temperature and retention time. The resulting SACs consist of disordered micrographite stacking, exhibiting good adsorption capacity for phenol, and the adsorption isotherms could be well fitted with the Langmuir equation. The results reveal the feasibility of SACs for removing organic pollutants from wastewater.

References

1. Sircar, S.; Golden, T. C.; Rao, M. B. Carbon 1996, 34, 1.
2. Magnuson, M. L.; Speth, T. F. Environ Sci Technol 2005, 39, 7706.
3. Popescu, M.; Joly, J. P.; Carré, J.; Danatoiu, C. Carbon 2003, 41, 739.
4. Besson M.; Gallezot, P.; Perrard, A.; Pinel, C.; Catal Today 2005, 160, 102.
5. Frackowiak, E. Phys Chem Chem Phys 2005, 9, 1774.
6. de la Casa-Lillo, M. A.; Lamari-Darkrim, F.; Cazorla-Amoros, D.; Linares-Solano, A. J Phys Chem B 2002, 106, 10930.
7. Hu, Z.; Srinivasan, M. P.; Ni, Y. Carbon 2001, 39, 877.
8. Tennison, S. R. Appl Catal A Gen 1998, 173, 289.
9. Lenghaus, K.; Qiao, G. G.; Solomon, D. H.; Gomez, C.; Rodriguez-Reinoso, F.; Sepulveda-Escribano, A. Carbon 2002, 40, 743.
10. Oya, A.; Yoshida, S.; Alcaniz-Monge, J.; Linares-Solano, A. Carbon 1995, 33, 1085.
11. Teng, H.; Wang, S.-C. Ind Eng Chem Res 2000, 39, 673.
12. Yue, Z.; Economy, J.; Bordson, G. J Mater Chem 2006, 6, 1456.
13. Wang, Y. X.; Tan, S. H.; Jiang, D. L.; Zhang, X.Y. Carbon 2065 2003, 41.
14. Tamai, H.; Kouzu, M.; Yasuda, H. Carbon 2003, 41, 1678.
15. Huang, J.-M.; Wang, I.-D.; Wang, C.-H. J Polym Res 2001, 8, 201.
16. Tanaike, O.; Hatori, H.; Yamada, Y.; Shiraishi, S.; Oya, A. Carbon 2003, 41, 1759.
17. La'szlo', K. Micropor Mesopor Mater 2005, 80, 205.
18. Sun, J.; Wu, G.; Wang, Q. J Appl Polym Sci 2004, 93, 602.
19. Yang, J. B.; Ling, L. C.; Liu, L.; Kang, F. Y.; Huang, Z. H.; Wu, H. Carbon 2002, 40, 911.
20. Li, A.; Zhang, Q.; Zhang, G.; Chen, J.; Fei, Z.; Liu, F. Chemosphere 2002, 47, 981.
21. Gregg, S. J.; Sing, K. S. Adsorption, Surface Area and Porosity; Academic Press: London, 1982.
22. Zhang, S.-J.; Yu, H.-Q.; Feng, H.-M. Carbon 2059 2006, 44.
23. Munoz-Guillena, M. J.; Illan-Gomez, M. J.; Martin-Martinez, J. M.; Linares-Solano, A.; Salinas-Martinez de Lecea, C. Energ Fuel 1992, 6, 9.
24. Wang, S.; Lu, G. Q. Ind Eng Chem Res 1997, 36, 5103.
25. Lua, A. C.; Yang, T. J Colloid Interface Sci 2004, 274, 594.
26. Gonzalez-Serrano, E.; Cordero, T.; Rodriguez-Mirasol, J.; Cotoruelo, L.; Rodriguez, J. J. Water Res 2004, 38, 3043.
27. Warhurst, A. M.; McConnachie, G. L.; Pollard, S. J. T. Water Res 1997, 31, 759.
28. Tseng, R. L.; Wu, F. C.; Juang, R. S. Carbon 2003, 41, 487.
29. Laszlo, K.; Podkoscielny, P.; Dabrowski, A. Langmuir 2003, 19, 5287.